






<https://doi.org/10.1038/s42003-021-02696-9>

OPEN

The application of tissue-engineered fish swim bladder vascular graft

Hualong Bai ^{1,2}✉, Peng Sun¹, Haoliang Wu¹, Shunbo Wei¹, Boao Xie¹, Wang Wang^{2,3}, Yachen Hou⁴, Jing'an Li ⁴✉, Alan Dardik ^{5,6}✉ & Zhuo Li ^{2,7}✉

Small diameter (<6 mm) prosthetic vascular grafts continue to show very low long-term patency, but bioengineered vascular grafts show promising results in preclinical experiments. To assess a new scaffold source, we tested the use of decellularized fish swim bladder as a vascular patch and tube in rats. Fresh goldfish (*Carassius auratus*) swim bladder was decellularized, coated with rapamycin and then formed into patches or tubes for implantation in vivo. The rapamycin-coated patches showed decreased neointimal thickness in both the aorta and inferior vena cava patch angioplasty models. Rapamycin-coated decellularized swim bladder tubes implanted into the aorta showed decreased neointimal thickness compared to uncoated tubes, as well as fewer macrophages. These data show that the fish swim bladder can be used as a scaffold source for tissue-engineering vascular patches or vessels.

¹Department of Vascular and Endovascular Surgery, First Affiliated Hospital of Zhengzhou University, Henan, China. ²Key Vascular Physiology and Applied Research Laboratory of Zhengzhou City, Henan, China. ³Department of Physiology, Medical school of Zhengzhou University, Henan, China. ⁴School of Material Science and Engineering & Henan Key Laboratory of Advanced Magnesium Alloy & Key Laboratory of materials Processing and Mold Technology (Ministry of Education), Zhengzhou University, Henan, China. ⁵The Vascular Biology and Therapeutics Program, Yale School of Medicine, New Haven, CT, USA. ⁶Departments of Surgery and of Cellular and Molecular Physiology, Yale School of Medicine, New Haven, CT, USA. ⁷Department of Neurology, First Affiliated Hospital of Zhengzhou University, Henan, China. ✉email: baihualongdoctor@126.com; lijingan@zzu.edu.cn; alan.dardik@yale.edu; zhuolimarch@126.com

Small diameter (<6 mm) vascular grafts continue to show very low long-term patency after surgery¹, with >50% of patients requiring major amputation within a year after failure of an infrageniculate bypass graft². Although polyester and expanded polytetrafluoroethylene vascular grafts have been widely used for more than half a century^{3,4}, they do not have acceptable long-term patency and therefore autogenous blood vessels remain the preferred choice of conduit due to their higher patency rate⁵, especially when a ‘no touch’ vein graft harvesting technique is used⁶. Although autogenous vein has satisfactory long-term patency, some patients who need bypass surgery do not have suitable autologous vein; diameter mismatch between the autogenous vein and host vessel remains problematic, and spiral vein grafts are rarely used since they are technically demanding.⁷ Accordingly, several biological vascular grafts have been developed for clinical use, including cryopreserved allografts⁸, human umbilical vein grafts⁹, and xenografts^{10,11}. Xenogeneic tissue can be used as a bioengineered vascular scaffold^{12,13}, and several commonly used xenogeneic decellularized patches derived from porcine or bovine pericardium are commercially available. Similar to the transition from the first generation of prosthetic materials to the current advanced polymer fabric grafts, the progress in the fields of physiology, cell biology, and biomanufacturing over the past several decades, coupled with recent advances in the tissue-engineering, suggest that next-generation tissue-engineered vascular grafts may become the mainstays of surgical therapy for vascular disease¹⁴.

Decellularized xenogeneic vascular scaffolds retain the extracellular matrix to maintain the overall shape and architecture of a structure but have fewer immunological reactions due to the decellularization process. Since chitosan extracted from the shells of crab and shrimp appears to be a promising material¹⁵, we speculated that some organs in bony fish could be similarly processed and used as a scaffold for clinical use. The goldfish *Carassius auratus* is a very common type of fish in China, with high availability. Collagen extracted from fish swim bladders or shark cartilage is similar to mammalian collagen^{16–18}; the swim bladder is composed of collagens, elastin, glycosaminoglycan¹⁹; and may be a potential source for arterial scaffolds. In China, fisheries routinely discard the goldfish swim bladder; each 700–800 g fresh water fish can yield a 5–7 cm swim bladder, suggesting a sustainable source for collagen-based scaffolds.

Fish swim bladder is rarely considered for study in vascular research, with only one reported study; Liu et al.²⁰ showed less

calcification of fish swim bladder compared with bovine pericardium both in vitro and in vivo, as well as higher patency and lower calcification in a rat arterial model, suggesting that fish swim bladder is a potential candidate cardiovascular biomaterial. However, whether fish swim bladder can be used in the venous system or as a patch, is not known; in addition, it is also not known whether the surface of the fish swim bladder can be coated with a therapeutic drug, and surface modification is currently an important area for research and development²¹. Rapamycin is an effective drug that is widely used to inhibit neointimal hyperplasia both in clinical²² and in basic research^{23,24}. Previously we showed that pericardial patches can be coated with rapamycin-containing nanoparticles to inhibit neointimal hyperplasia²³. The decellularized pericardial patch²³, decellularized human saphenous vein patch²⁵, and rat thoracic aorta patch^{26,27} can also be coated with heparin or PD-1 antibody to decrease neointimal thickness. We hypothesized that decellularized fish swim bladder can serve as a biological vascular graft scaffold and can be surface modified; accordingly, we created swim bladder-derived scaffolds, coated them with rapamycin, shaped them into patches or tubes, and implanted them into rats to determine biocompatibility.

Results

We assessed the biocompatibility of the fish swim bladder as a source of collagen-based scaffolds (Fig. 1); since the fish swim bladder would be used as a xenograft, to decrease the chance of immunological rejection, we decellularized the swim bladder and examined it, without any additional coating. Hematoxylin and eosin (H&E) staining showed lack of cell nuclei between the wavy collagen fibers (Fig. 2a, b); Verhoeff-Van Gieson (EVG) and trichrome staining, Safranin O, and Sirius Rosa BB staining showed preservation of elastin and collagen fibers after decellularization (Fig. 2a and Supplementary Fig. 1a); Alizarin Red S staining showed no obvious calcification in native and decellularized patches (Supplementary Fig. 1a). Immunofluorescence confirmed lack of any residual cells (Supplementary Fig. 1b), and the DNA content dropped to almost zero after decellularization (Supplementary Fig. 1c). Immunohistochemistry showed α -actin, collagen-1, fibronectin and vimentin were positive stained before decellularization (Fig. 2a); after decellularization there were no α -actin- or vimentin-positive cells, but collagen-1 and fibronectin were preserved. This data shows that decellularization was effective in the fish swim bladder.

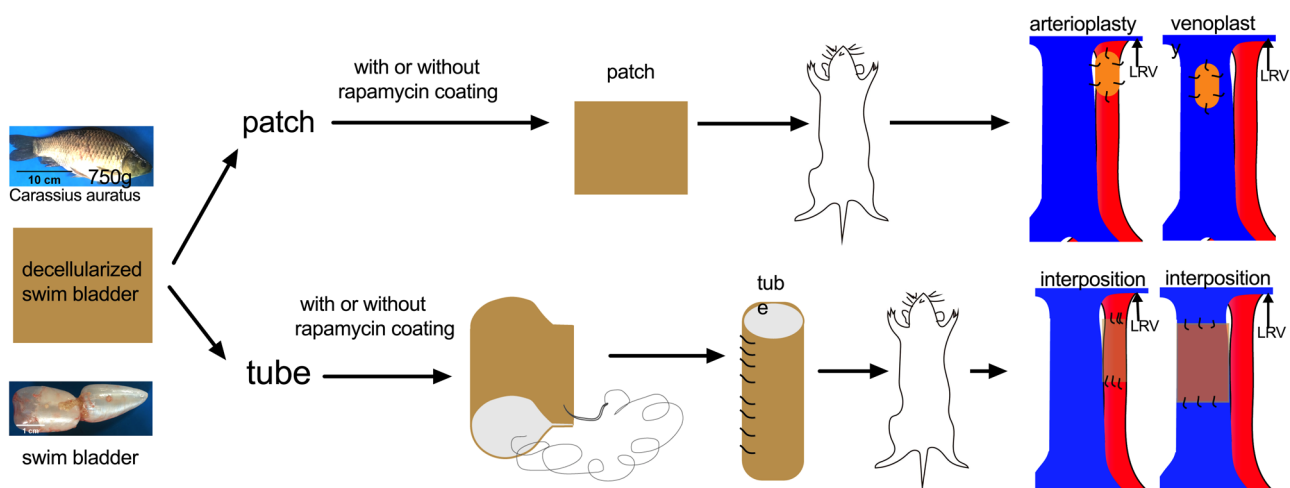


Fig. 1 Illustration showing the overall experimental design. LRV, left renal vein. This illustration was created by Dr. Hualong Bai.

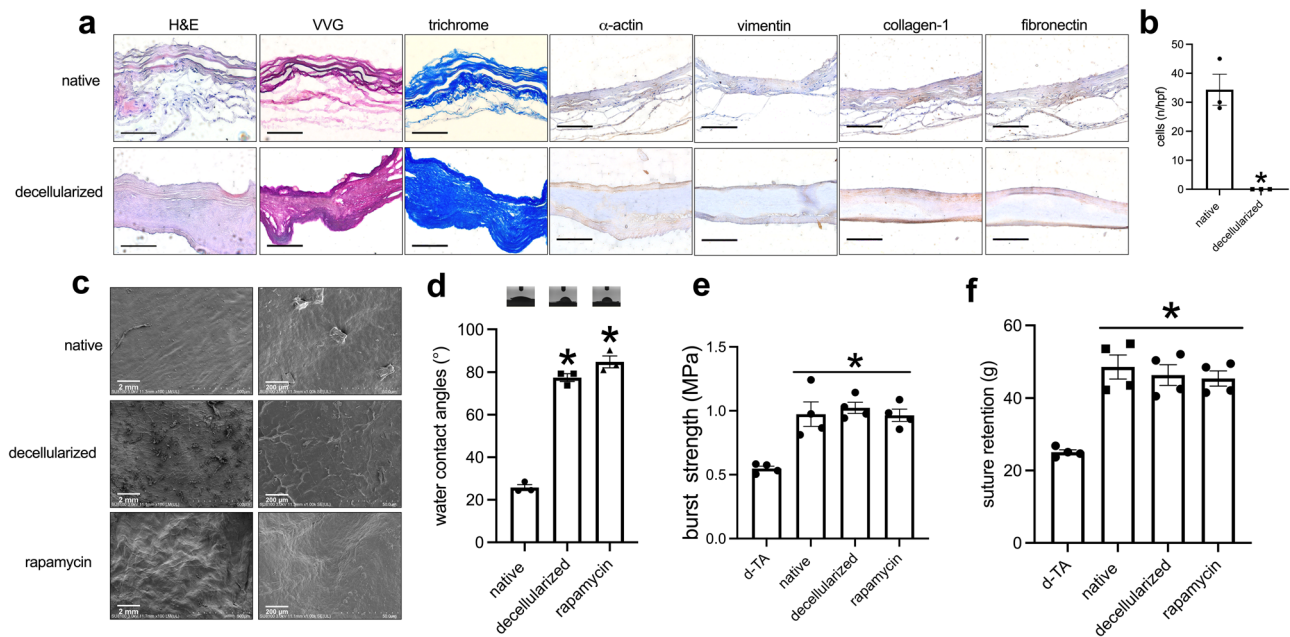


Fig. 2 Comparison of the fresh and decellularized fish swim bladder. **a** Photographs showing the swim bladder before and after decellularization, stained with hematoxylin & eosin, VVG, trichrome, α -actin, collagen-1, fibronectin, or vimentin; scale bar, 100 μ m; $n = 3$. **b** Bar graph showing the cell number before and after decellularization, $*p = 0.0031$, t -test; $n = 3$. **c** SEM images of fresh, decellularized and rapamycin-coated patches (rapa-coating); scale bar, 200 μ m; $n = 3$. **d** Water contact angles of fresh, decellularized and rapamycin-coated patches; the inset panels showing the photographs of the water contact angles; $p < 0.0001$, one-way ANOVA; $*p < 0.0001$, Tukey's multiple comparisons test; $n = 3$. **e** Bar graph showing the burst test, $*p = 0.0003$, one-way ANOVA; d-TA, decellularized rat thoracic aorta; $n = 4$. **f** Bar graph showing the suture retention, $*p < 0.0001$, one-way ANOVA; d-TA, decellularized rat thoracic aorta; $n = 4$. Data are expressed as mean \pm s.e.m.

To see if the surface of swim bladder could be modified, rapamycin was coated onto the surface of swim bladder. Scanning electron microscopy (SEM) showed a smooth surface before decellularization but a rough surface after decellularization; with rapamycin coating, the surface was a smooth pattern (Fig. 2c). To see the hydrophilic property of surface after modification, water contact angle (WCA) was measured in patches of swim bladder; in the native swim bladder, there was a smaller WCA; after decellularization, there was much larger WCA, and there was no significant difference between the decellularized and rapamycin-coated swim bladder (Fig. 2d). There was a similar burst pressure and suture retention among the native, decellularized and rapamycin-coating patches, with increased burst pressure and suture retention compared to decellularized rat thoracic aorta (d-TA) (Fig. 2e, f). Rapamycin was released for up to 14 days in vitro (Supplementary Fig. 2a). Nanoparticles containing rhodamine (Supplementary Fig. 2b) showed release for up to 24 hours in vivo (Supplementary Fig. 2c). These data show that the decellularized swim bladder can be successfully coated with rapamycin without loss of structural integrity, suggesting suitability for testing in vivo.

We also examined HUVEC apoptosis on the control and hyaluronic acid-rapamycin-coated fish patches. Cells had detectable fluorescence after AO/EB staining, with viable HUVEC showing green color and apoptotic HUVEC showing red color; both the control decellularized fish patches and hyaluronic acid-rapamycin-coated decellularized fish patches showed more viable HUVEC (green) than apoptotic HUVEC (red), and also showed increased numbers of HUVEC over time (Supplementary Fig. 3a). Hyaluronic acid-rapamycin-coated decellularized fish patch had an increased HUVEC vital ratio compared with control decellularized fish swim bladder (Supplementary Fig. 3b). Both patches promoted HUVEC adhesion and proliferation, while hyaluronic acid-rapamycin-coated

decellularized fish patches showed better function compared with control patches (Supplementary Fig. 3c, d).

We also examined decellularized fish swim bladder patches with or without rapamycin conjugation implanted subcutaneously or into the abdominal cavity; cells migrated and infiltrated into the patch at days 1, 3 and 7, and the number of infiltrated cells increased over time (Supplementary Fig. 4).

Patches. We tested the application of the decellularized swim bladder without or with rapamycin coating as patches placed into the rat aorta or the IVC^{25,26,28,29}. At day 14, the patches were incorporated into the rat aorta and IVC; there were no aneurysms or occlusions. H&E and EVG staining showed a much thinner neointima in the rapamycin-coated patches compared to the decellularized swim bladder patches (Fig. 3a, b and Supplementary Fig. 5a); immunohistochemistry showed some α -actin-positive cells in the neointima (Supplementary Fig. 5a). There was also less newly formed adventitia on the outer side of the rapamycin-coated patches (Fig. 3a, c), and fewer cells infiltrated into the interspace between the swim bladder fibers in the rapamycin-coated patches (Fig. 3a, d). Immunohistochemistry and immunofluorescence showed a line of CD31 and CD34-positive cells on the luminal surface of the neointima; there was no difference in the amount of reendothelialization or percentage of CD34-positive cells between the control and rapamycin-coated patches (Fig. 4a–e). Within the tissue that formed on the adventitial surface, there were increased numbers of CD31-positive cells, consistent with new capillaries, and there were fewer CD31-positive cells in the rapamycin-coated patches compared to the control patches (Fig. 4f, g and Supplementary Fig. 5b). There were similar percentages of Ephrin-B2 and Dll-4-positive cells on the luminal surface of the neointima in the arterioplasty patches (Fig. 4h, i and Supplementary Fig. 6). There were also similar percentages of Eph-B4 and COUP-TFII-positive

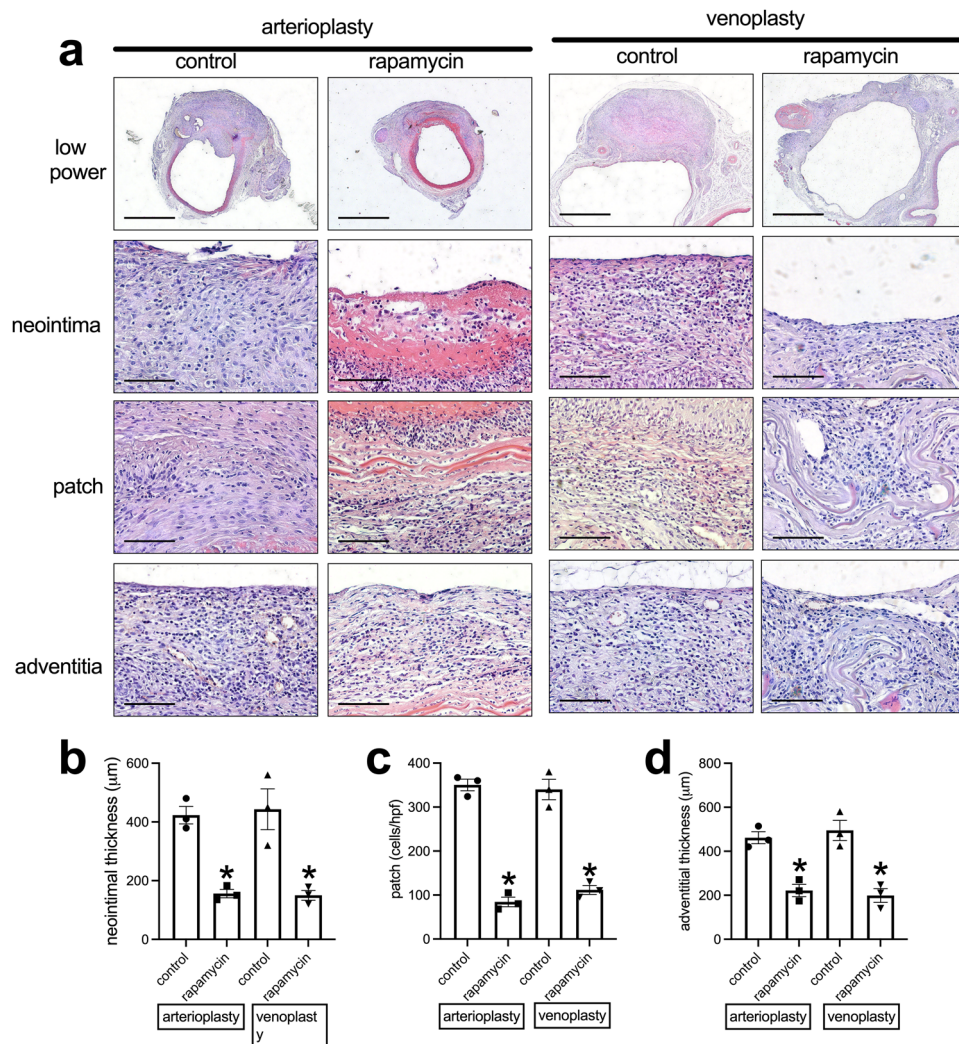


Fig. 3 Swim bladder patches harvested from aorta arterioplasty and IVC venoplasty at day 14. **a** Photographs of hematoxylin & eosin staining of the swim bladder patches after arterioplasty or venoplasty, day 14. First row, low power photographs, scale bar, 1 mm; second to fourth rows, high-power photographs shows the neointima, cells infiltrated into the patch and the newly formed adventitia; scale bar, 100 µm; $n = 3$. **b** Bar graph showing the neointimal thickness in the arterioplasty ($*p = 0.013$) and venoplasty ($*p = 0.0147$) models, day 14; t -test; $n = 3$. **c** Bar graph showing the cells infiltrated into the patch in the arterioplasty ($*p = 0.0001$) and venoplasty ($*p = 0.0008$) models, day 14; t -test; $n = 3$. **d** Bar graph showing the adventitial thickness in the arterioplasty ($*p = 0.0037$) and venoplasty ($*p = 0.0059$) models, day 14; t -test; $n = 3$. Data are expressed as mean \pm s.e.m.

cells on the luminal surface of the neointima in the venoplasty patches (Fig. 4j, k and Supplementary Fig. 6). There were fewer PCNA-positive cells in the neointima in the rapamycin-coated patches compared to the control patches in the arterioplasty (Fig. 5a, b) and in the venoplasty (Fig. 5a, b) models. There were fewer CD68-positive cells in the neointima of the rapamycin-coated patches compared to the control patches in the arterioplasty and venoplasty models (Fig. 5c and Supplementary Fig. 7). There were similar numbers of CD68 and IL-10 dual-positive cells, CD68 and TGM2 dual-positive cells, CD68 and iNOS dual-positive cells, and CD68 and TNF α dual-positive cells in the neointima of the rapamycin-coated patches compared to the control patches in the arterioplasty (Fig. 5d–g and Supplementary Fig. 7a). However, in venoplasty, there were similar amount of CD68 and IL-10 dual-positive cells, but fewer CD68 and TGM2 dual-positive cells, similar CD68 and iNOS dual-positive cells, and fewer CD68 and TNF α dual-positive cells in the neointima of the rapamycin-coated patches compared to the control patches (Fig. 5d–g and Supplementary Fig. 7b). These data showed that decellularized swim bladder can be used as a tissue-engineered vascular patch in both the arterial and

venous environments and coated with rapamycin to decrease local neointimal thickening.

Tubes. Since vascular grafts are commonly used for bypass surgeries, we also examined whether swim bladder can be used in a tube configuration. Tubes were made of decellularized bladder by rolling the swim bladder and suturing it with a double layer of sutures (Fig. 6a); tubes of 1 mm diameter were used as aortic interposition grafts and tubes of 2 mm diameter were used as IVC interposition grafts. After implantation, the tube grafts showed good strength without leakage, in both the aorta and IVC (Fig. 6b). After 14 days, all aortic tube grafts were patent; all three IVC tube grafts were occluded in the control group, while the rapamycin-coated tube grafts were all patent (Fig. 6c, d). H&E and EVG staining showed a significantly thinner neointima on the luminal surface of the grafts in the aorta and IVC positions (Fig. 6d, e and Supplementary Fig. 8a). There were also fewer cells infiltrated into the patch of the rapamycin-coated tube grafts compared to the control tube grafts (Fig. 6d, f). There was also a

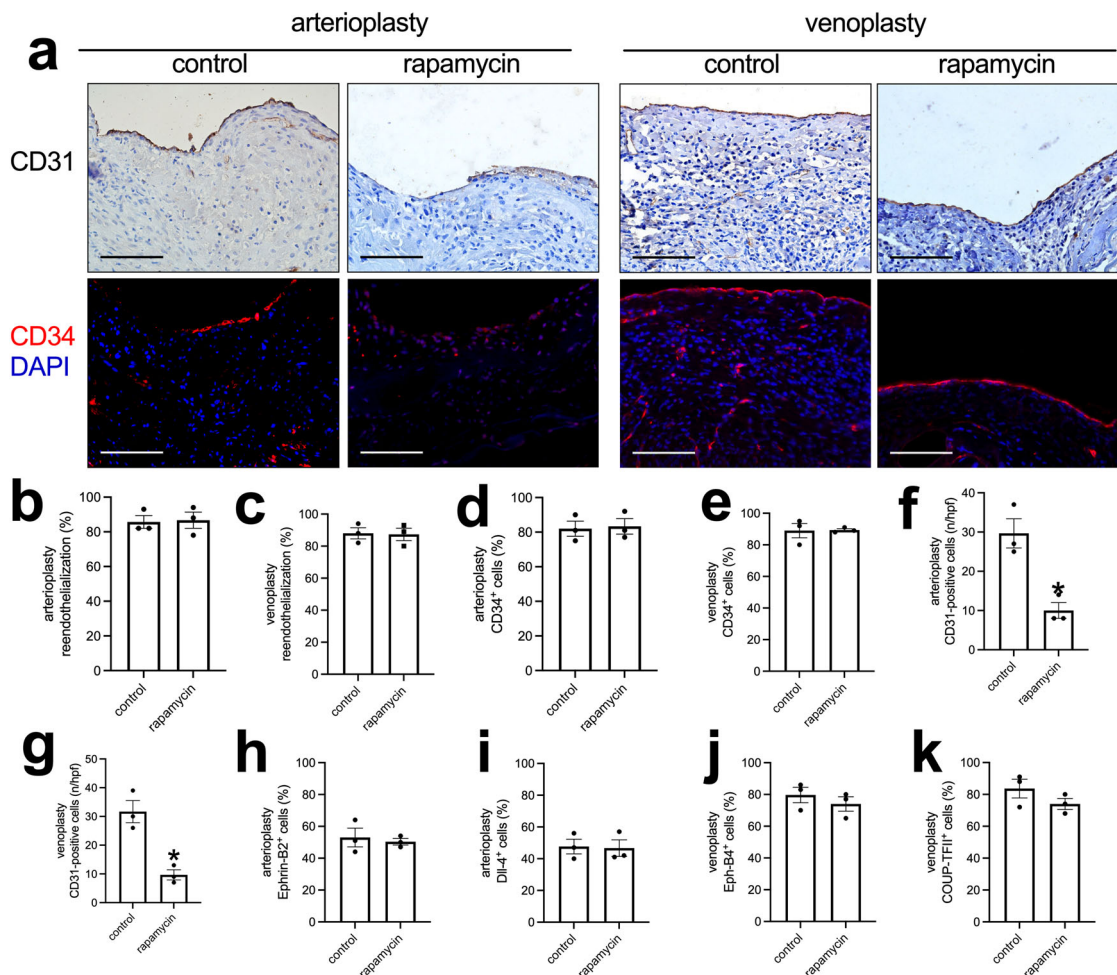


Fig. 4 Endothelial cell identity in the control or rapamycin-coated patches harvested from aorta arterioplasty or IVC venoplasty, day 14. **a** First row, Photograph of immunohistochemistry stained for CD31; second row, and photograph of the immunofluorescence merge of CD34 (red) and DAPI (blue) of the neointima; scale bar, 100 μ m, $n = 3$. **b, c** Bar graphs showing neointimal reendothelialization of the arterioplasty ($p = 0.8744$) and venoplasty ($p = 0.9037$), day 14; t -test; $n = 3$. **d, e** Bar graphs showing the neointimal CD34-positive cell coverage in the arterioplasty ($p = 0.8416$) and venoplasty ($p = 0.9465$) model at day 14, t -test, $n = 3$. **f, g** Bar graphs showing the adventitial CD31-positive cells in the arterioplasty ($*p = 0.0096$) and venoplasty ($*p = 0.0065$), day 14; t -test; $n = 3$. **h, i** Bar graphs showing the percentages of neointimal Ephrin-B2 ($p = 0.6893$) and dll-4 ($p = 0.8925$) positive cells in the arterioplasty, day 14; t -test; $n = 3$. **j, k** Bar graphs showing the percentages of neointimal Eph-B4 ($p = 0.4463$) and COUP-TFII ($p = 0.2304$) positive cells in the venoplasty, day 14; t -test; $n = 3$. Data are expressed as mean \pm s.e.m.

thinner adventitia in the rapamycin-coated tube grafts compared to the control tube grafts (Fig. 6d, g). Immunohistochemistry showed some α -actin-positive cells in the neointima (Supplementary Fig. 8a).

Immunohistochemistry and immunofluorescence showed a layer of CD31 and CD34-positive cells on the luminal surface of the neointima except control tube graft in the IVC (Fig. 7a–e). In the adventitial surface of the tube grafts, there were increased numbers of CD31-positive cells, consistent with new capillaries, and there were fewer CD31-positive cells in the rapamycin-coated tube grafts compared to the control tube grafts (Fig. 7f, g and Supplementary Fig. 8b). There were Ephrin-B2 and Dll-4-positive cells on the luminal surface of the neointima on the luminal surface of the aortic tube grafts (Fig. 7h, i and Supplementary Fig. 9); the Ephrin-B2 and dll-4-positive cells on the luminal surface of the neointima on the rapamycin-coated tube grafts appeared more continuous compared to the control grafts (Supplementary Fig. 9). There were more Eph-B4 and COUP-TFII-positive cells in the rapamycin-coated tube grafts compared to the control tube grafts in the IVC (Fig. 7j, k and Supplementary Fig. 9). There were fewer PCNA-positive cells in the neointima of

the rapamycin-coated tube grafts compared to the control tube grafts in both the aorta and IVC (Fig. 8a, b). There were fewer CD68-positive cells in the neointima of the rapamycin-coated tube grafts compared to the control tube grafts in the aorta and the IVC (Fig. 8c). There were also fewer CD68 and IL-10 dual-positive cells, fewer CD68 and TGM2 dual-positive cells, fewer CD68 and iNOS dual-positive cells, and fewer CD68 and TNF α dual-positive cells in the neointima of the rapamycin-coated tube grafts compared to the control tube grafts in both the aorta and IVC (Fig. 8d–g and Supplementary Fig. 10a, b). These data show that the decellularized swim bladder can be fashioned as a tube and used in both the arterial and venous environments and coated with rapamycin to decrease local neointimal thickening.

Discussion

Here, we show that decellularized fish swim bladder can be used as a vascular patch or as an interposition tube graft in both the rat IVC and the aorta, and thus successfully model the patch angioplasty and tube interposition grafts that are surgical procedures commonly used in vascular surgery^{7,29}. These decellularized fish swim bladder-based scaffolds can be coated with rapamycin to

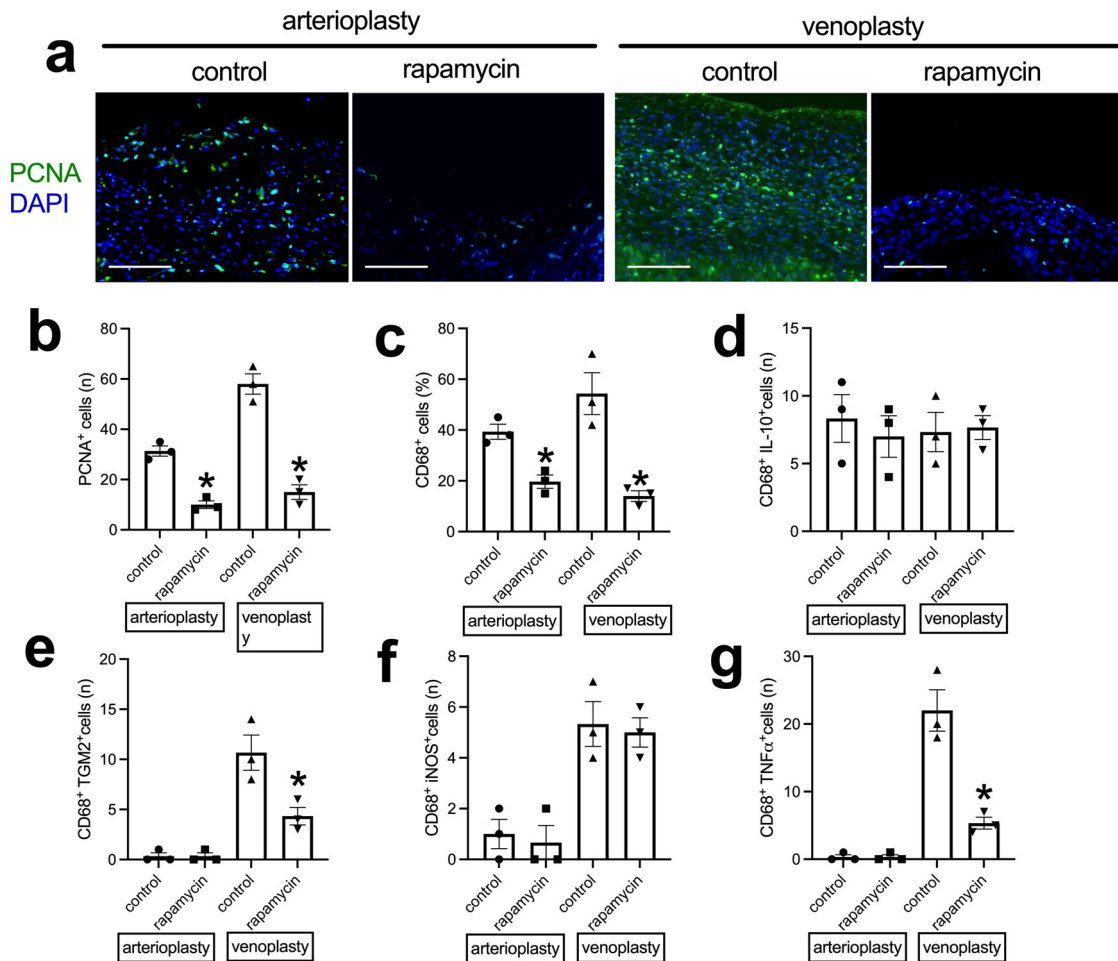


Fig. 5 Neointimal cell proliferation and macrophage identity in the control or rapamycin-coated patches harvested from aorta arterioplasty or IVC venoplasty, day 14. **a** Photograph of the immunofluorescence merged of PCNA (green) and DAPI (blue) of the patches; scale bar, 100 μ m; $n = 3$. **b** Bar graph showing the neointimal PCNA-positive cells in the control or rapamycin-coated patches in the arterioplasty ($*p = 0.0011$) or venoplasty ($*p = 0.0010$) models, day 14; t -test; $n = 3$. **c** Bar graph showing the neointimal CD68-positive cells in the control or rapamycin-coated patches of the arterioplasty ($*p = 0.0076$) or venoplasty ($*p = 0.0090$) models, day 14; t -test; $n = 3$. **d** Bar graph showing the CD68 and IL-10 dual-positive cells in the control or rapamycin-coated patches in the arterioplasty ($p = 0.5983$) or venoplasty ($p = 0.8541$) models, day 14; t -test; $n = 3$. **e** Bar graph showing the CD68 and TGM2 dual-positive cells in the control or rapamycin-coated patches in the arterioplasty ($p > 0.9999$) or venoplasty ($*p = 0.0325$) models, day 14; t -test; $n = 3$. **f** Bar graph showing the CD68 and iNOS dual-positive cells in the control or rapamycin-coated patches in the arterioplasty ($p = 0.7247$) or venoplasty ($p = 0.7676$) models, day 14; t -test; $n = 3$. **g** Bar graph showing the CD68 and TNF- α dual-positive cells in the control or rapamycin-coated patches in the arterioplasty ($p > 0.9999$) or venoplasty ($*p = 0.0063$) models, day 14; t -test; $n = 3$. Data are expressed as mean \pm s.e.m.

inhibit both arterial and venous neointimal hyperplasia. These data show that the fish swim bladder can be used as a scaffold source for tissue-engineering vascular patches or vessels.

Tube grafts remain an essential tool for vascular reconstruction. Although native veins are preferred, and prosthetic grafts based on PTFE or polyester are commonly used, there are common clinical situations in which conduits would be preferred, including in the presence of infection or trauma; in addition, large vessels are frequently mismatched in diameter to native vessels such as saphenous vein. We tested the swim bladder in tube configuration in both the rat IVC and aorta; interestingly, all the tubes placed in the IVC were occluded, and all three rapamycin-coated tubes were patent; the lower flow in the venous system and platelet accumulation may have played a role in this process; in addition, the increased proliferation of neointimal cells and/or the larger number of macrophages and M2-type macrophages may have also contributed (Fig. 8). However, swim bladder tubes placed in the aorta were all patent, and there was with a thinner neointima in the grafts coated with rapamycin, suggesting that

decellularized fish swim bladder is a potential vascular graft scaffold that can be used for tissue-engineering. Compared to other commercially available prosthetic grafts and biological grafts, the structure of the decellularized fish swim bladder is more similar to native vessels, with increased mechanical strength and stability and excellent hemocompatibility²⁰. (Fig. 6).

Neointimal hyperplasia is still a persistent etiology of vascular graft restenosis and failure after vascular interventions³⁰, and rapamycin is a commonly used drug that inhibits neointimal hyperplasia in both the clinic as well as research studies^{23,24}. We show that decellularized fish swim bladder grafts can be coated with rapamycin and effectively inhibit neointimal hyperplasia in both patch angioplasty and tube interposition graft models (Figs. 3 and 6). Fewer cells infiltrated into the rapamycin-coated grafts, and fewer PCNA and CD68-positive cells were present in the rapamycin-coated grafts, suggesting limited remodeling (Figs. 5 and 8); this limited remodeling of rapamycin-coated grafts may have contributed to increased graft patency, and retention of the native elasticity and compliance. Boada et al.³¹

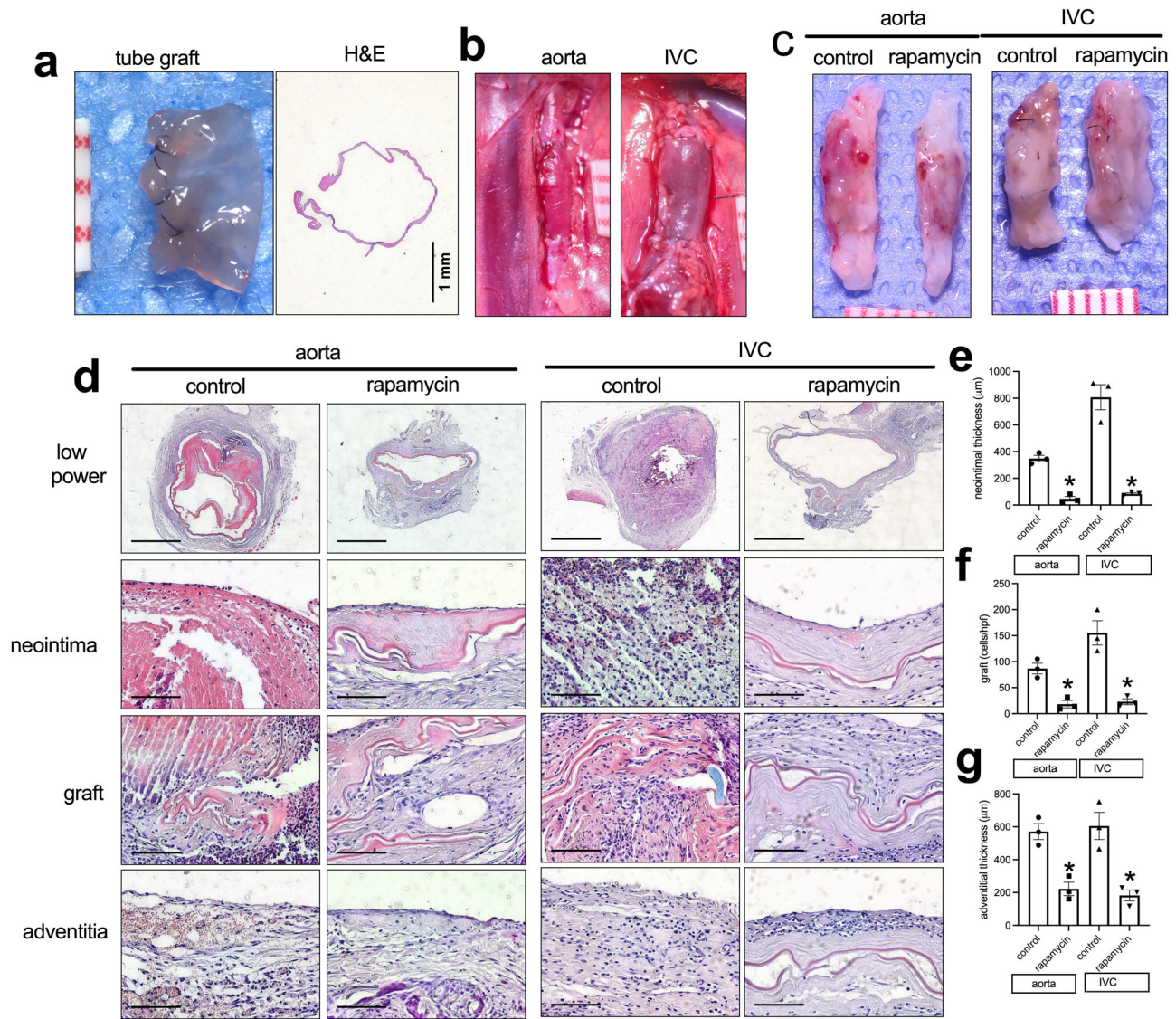


Fig. 6 Swim bladder used as a interposition tube graft in the aorta or IVC. **a** Photograph of a vascular tube made of decellularized swim bladder using 11-0 suture; ruler marks 1 mm; H&E staining of a swim bladder tube before implantation. **b** Photographs of swim bladder interposition tube graft in aorta and IVC after completion of the anastomoses; ruler marks 1 mm. **c** Photographs of swim bladder interposition tube grafts, ruler marks 1 mm, day 14. **d** H&E staining of the swim bladder tube grafts, day 14. First row, low power photographs; scale bar, 1 mm. second row, high-power photographs shows the neointima; scale bar, 100 µm; third row, high-power photographs shows the cells infiltrated into the swim bladder; scale bar, 100 µm; fourth row, high-power shows the newly formed adventitia; scale bar, 100 µm. **e** Bar graph showing the neointimal thickness in the aorta ($*p = 0.005$) and IVC ($*p = 0.0015$) interposition models, day 14; *t*-test; *n* = 3. **f** Bar graph showing the cells infiltrated into the interposition tube graft in the aorta ($*p = 0.0054$) and IVC ($*p = 0.0092$), day 14; *t*-test; *n* = 3. **g** Bar graph showing the adventitia; thickness in the aorta ($*p = 0.0055$) and IVC ($*p = 0.0053$) interposition models, day 14; *t*-test; *n* = 3. Data are expressed as mean \pm s.e.m.

showed that biomimetic rapamycin nanoparticles can suppress macrophage proliferation and depletion of macrophages could reduce neointimal hyperplasia^{32,33}. There were also fewer M2-type macrophages (dual-positive CD68 and IL-10, or dual-positive CD68 and TGM2), fewer M1-type macrophages (dual-positive CD68 and iNOS, or dual-positive CD68 and TNF α) in the neointima of the rapamycin-coated tube grafts compared to the control tube grafts in both the aorta and IVC (Figs. 5 and 8; and Supplementary Figs. 7 and 10); this suggests that both M1- and M2-type macrophages may contribute to neointimal hyperplasia in both the arterial and venous environments, which is similar to other studies^{34,35}. There were no differences in neointimal reendothelialization, CD34-positive cell number and endothelial cell identity between control grafts and rapamycin-coated grafts, which suggests that rapamycin coated onto fish

swim bladder grafts does not influence neointimal reendothelialization in both models, despite some studies that show rapamycin can delay neointimal reendothelialization^{36,37}. This inconsistency may be secondary to our studies being performed in a small rodent animal model.

There were several limitations in our research. First, we used fish swim bladders derived from fresh water goldfish, which are thinner and smaller than swim bladders derived from salt water fish; thicker swim bladders could give rise to other applications. Second, our research is limited to short time points and longer time points would give more data on longer term performance. Third, we used only a small animal model, and other large animal models that mimic human physiology more closely should also be tested. Fourth, the long-term comparison of fish swim bladder grafts with traditional vascular grafts needs be

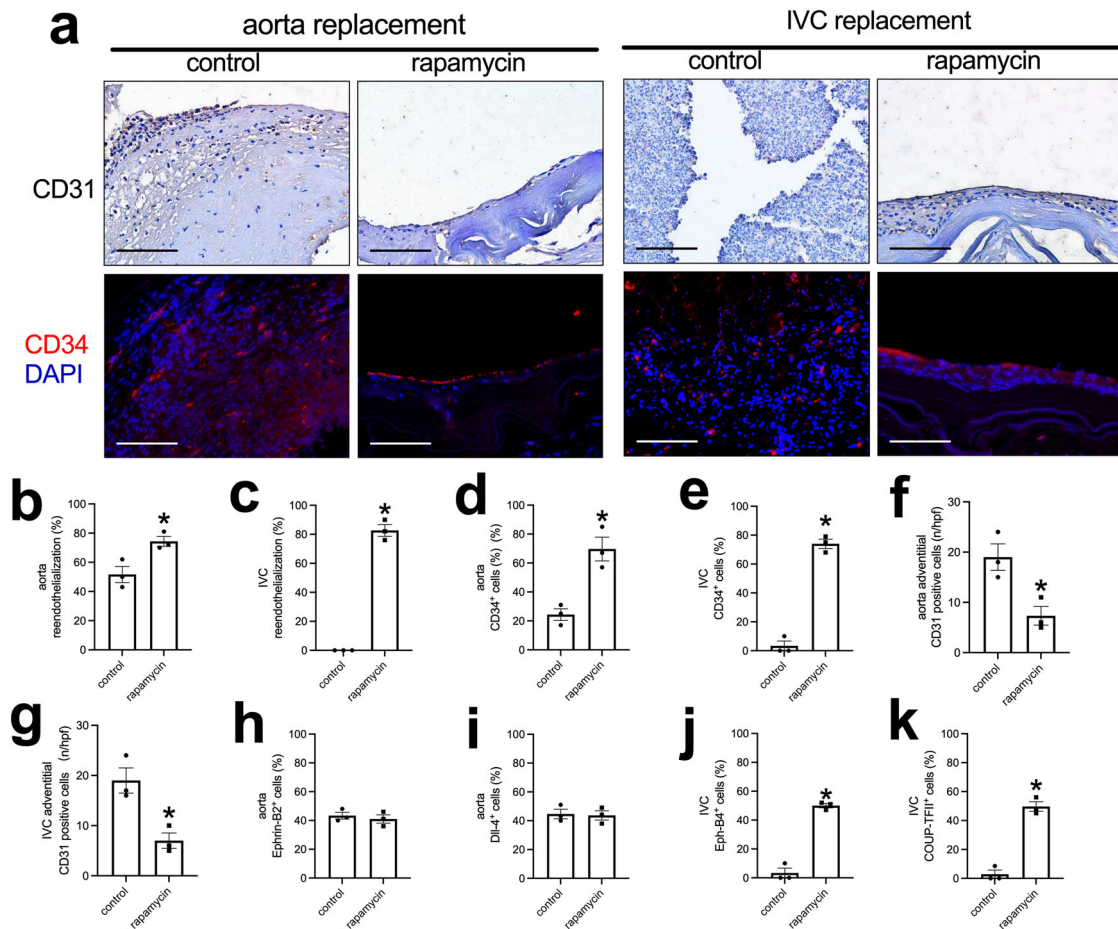


Fig. 7 Endothelial cell identity in the control or rapamycin-coated tube grafts harvested from aorta or IVC, day 14. **a** First row, Photograph of immunohistochemistry stained for CD31; second row, and photograph of the immunofluorescence merged of CD34 (red) and DAPI (blue) of the neointima in the tube graft; scale bar, 100 μ m, $n = 3$. **b, c** Bar graph showing the neointimal reendothelialization of the aortic tube graft ($*p = 0.0252$) and IVC ($*p < 0.0001$) tube graft models, day 14; t -test; $n = 3$. **d, e** Bar graph showing the percentage of CD34-positive cells in the aortic ($*p = 0.0077$) or IVC ($*p = 0.0001$) tube grafts, day 14; t -test; $n = 3$. **f, g** Bar graphs showing the adventitial CD31-positive cells of the aorta ($*p = 0.0226$) and IVC tube graft ($*p = 0.0151$) models, day 14; t -test; $n = 3$. **h, i** Bar graph showing the percentage of neointimal Ephrin-B2 ($p = 0.6965$) and dII-4 ($p = 0.9404$) positive cells in the neointima of the aortic tube grafts, day 14; t -test; $n = 3$. **j, k** Bar graphs showing the percentage of neointimal Eph-B4 ($*p = 0.0002$) and COUP-TFII ($*p = 0.0004$) positive cells in the neointima of the IVC tube grafts, day 14; t -test; $n = 3$. Data are expressed as mean \pm s.e.m.

tested. Fifth, given the high elasticity of the fish swim bladder, the application of fish swim bladder as an arteriovenous graft could also be explored.

We also showed that cells migrated and infiltrated into the decellularized fish swim bladder patch in a process similar to our previous observations that cells infiltrated into pericardial patches^{23,38}, polyester patches²⁹, decellularized human saphenous vein patches²⁵ and decellularized rat thoracic aortic patches²⁶. Also similar to other biomaterials, there was rapid reendothelialization after patch implantation or tube interposition; there were no patch pseudoaneurysms after aortic patch angioplasty, suggesting the structural strength and biocompatibility with the arterial environment (Fig. 4). Since the swim bladder-based patches are elastic, there is likely less compliance mismatch compared to prosthetic patches, minimizing anastomotic pseudoaneurysm formation³⁹; however, we only observed implantation for 14 days, a short duration of observation, and a longer time of observation is needed to detect longer term compatibility.

The decellularized swim bladder has previously been shown to have anti-calcification properties and excellent hemocompatibility when rolled into multi-layer tubes²⁰. Our data confirms these findings and extends these findings to show that surface modification of the scaffold with rapamycin inhibits neointimal

formation, a finding of translational significance. Modification of the surface of vascular grafts has showed the ability to inhibit neointimal hyperplasia, and surface modification with heparin⁴⁰ and collagen⁴¹ have both been used in human vascular surgery. Thus, surface modification of fish swim bladder-based scaffolds is likely to be a promising choice for future applications.

In summary, decellularized fish swim bladder can both be used as patches and tubes in rats, supporting endothelial cell migration and proliferation in vitro and in vivo. The decellularized fish swim bladder is a promising collagen-based scaffold that may be translated to human therapy, including using it for surface coating or modification to inhibit neointimal hyperplasia.

Methods

The study was approved by the First Affiliated Hospital of Zhengzhou University, Animal Care and Use Committee. All animal care complied with the Guide for the Care and Use of Laboratory Animals. NIH guidelines for the care and use of laboratory animals (NIH Publication #85-23 Rev. 1985) were observed.

Scaffold decellularization and coating. Fresh water goldfish (*Carassius auratus*) swim bladders were collected from a local market (Zhengzhou city, Henan Province, China). The swim bladder was stored in normal saline containing penicillin (100 U/mL) and streptomycin (100 μ g/mL) on ice after harvest and delivered immediately to the laboratory. The fat around the swim bladder can be easily dissected and removed

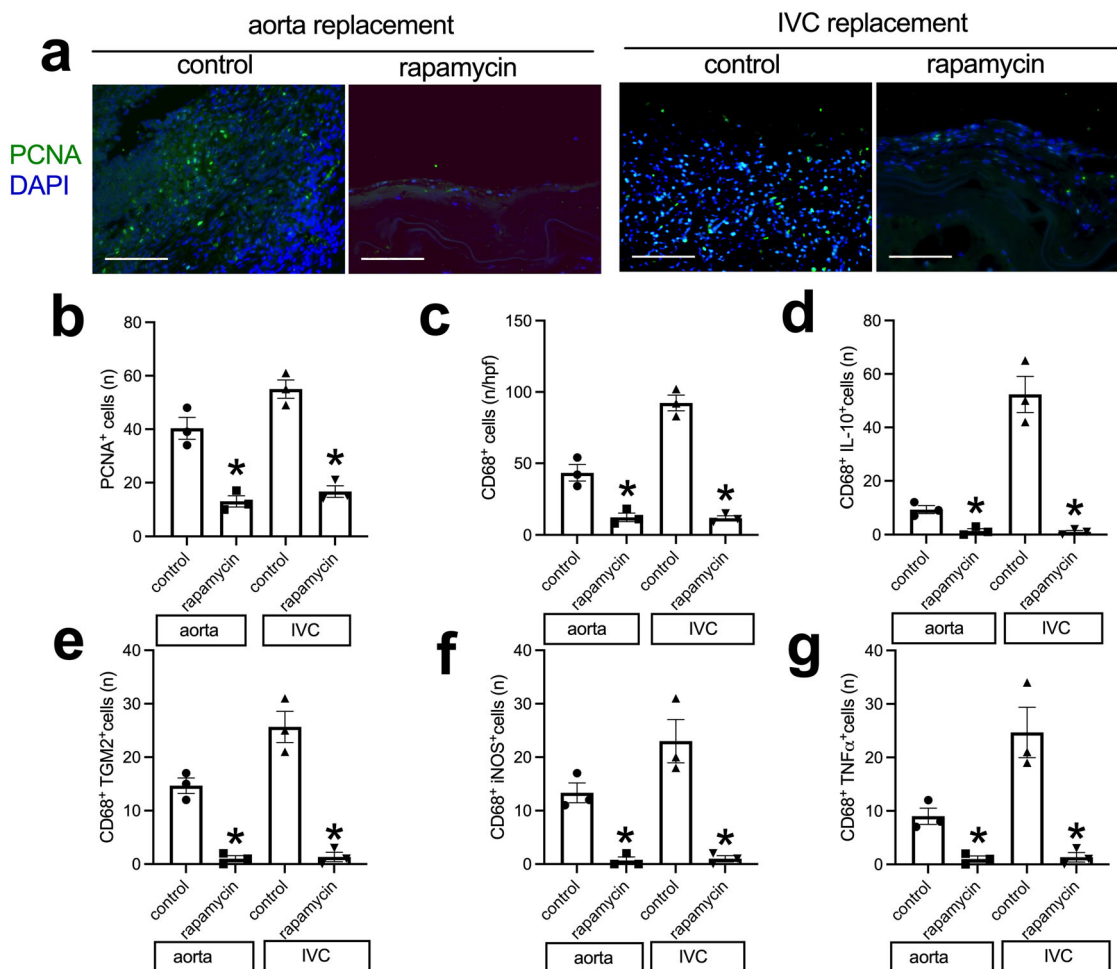


Fig. 8 Neointimal cell proliferation and macrophage plasticity in the control or rapamycin-coated tube grafts harvested from aorta or IVC, day 14. a Photograph of the immunofluorescence merged of PCNA (green) and DAPI (blue) of the neointima in the tube graft; scale bar, 100 μ m; $n = 3$. **b** Bar graph showing the PCNA-positive cells of the aortic ($*p = 0.0040$) or IVC ($*p = 0.0007$) tube grafts, day 14; t -test; $n = 3$. **c** Bar graph showing the neointimal CD68-positive cells in the control or rapamycin-coated tube grafts in the aorta ($*p = 0.0090$) or IVC ($*p = 0.0002$), day 14; t -test; $n = 3$. **d** Bar graph showing the number of CD68 and IL-10 dual-positive cells in the aortic ($*p = 0.0093$) or IVC ($*p = 0.0016$) tube grafts, day 14; t -test; $n = 3$. **e** Bar graph showing the number of neointimal CD68 and TGM2 dual-positive cells in the neointima of the aortic ($*p = 0.0009$) or IVC ($*p = 0.0013$) tube grafts, day 14. **f** Bar graph showing the number of neointimal CD68 and iNOS dual-positive cells in the neointima of the aortic ($*p = 0.0030$) or IVC ($*p = 0.0057$) tube grafts, day 14. **g** Bar graph showing the number of neointimal CD68 and TNF- α dual-positive cells in the neointima of the aortic ($*p = 0.0080$) or IVC ($*p = 0.0082$) tube grafts, day 14. Data are expressed as mean \pm s.e.m.

using a dissecting microscope (Nikon, Japan). Decellularization was performed; briefly, the swim bladder was incubated in 250 mL CHAPS buffer (8 mM CHAPS, 1 M NaCl, and 25 mM EDTA in PBS) for 12 h, followed by a 60 min wash, and then incubated in 10 mL sodium dodecyl sulfate buffer (1.8 mM sodium dodecyl sulfate, 1 M NaCl, and 25 mM EDTA in PBS) for 24 h, followed by wash with PBS to completely remove the detergent^{25,42}. Decellularized swim bladder scaffolds were then used for coating or for implantation. The rat thoracic aorta was harvested and decellularized in a similar fashion.

Swim bladders that were coated with rapamycin were immersed into a hyaluronic acid (HA) solution and coated⁴³. Briefly, after washing 3 times with phosphate-buffered saline (PBS; 5 min/wash), the HA-coated samples were immersed into a rapamycin solution (2 mg/mL; Zhaoke, Hefei, China) that was also advanced-activated in water-soluble carbodiimide solution (15 min), and incubated at 37 °C for 6 h⁴⁴. Rhodamine conjugation was carried out in a similar fashion²⁶.

Assessment of rapamycin bonding and release. To show that rapamycin was bonded to the surface of the decellularized swim bladder, we measured the water contact angles (WCA) of the decellularized swim bladder before and after rapamycin bonding, the WCA was measured on the hyaluronic acid rapamycin-coated decellularized swim bladder; morphology was assessed with SEM⁴⁵. Patches conjugated with nanoparticle rapamycin were incubated in PBS at 37 degrees, and the supernatant of each sample was collected and absorption (400 nm) was analyzed at each time point using a SpectraMax plate reader (Molecular Devices, Sunnyvale, CA).

Suture retention and burst test. Suture retention of the decellularized patches were measured⁴⁶. Briefly, suture retention testing was performed on rectangular specimens (5 cm \times 3 cm) clamped at the edges and located opposite to an 8-0 Prolene suture anchored 5 mm from the edge; the suture loop was pulled with a tension meter, and when the suture tore through the patch, the tension was recorded. The burst test measured the pressure at which the swim bladder burst when connected to a calibrated inflation device (BasixCompak, Merit Medical, 30 atm maximum pressure). Uniaxial testing was not performed since it has been previously reported²⁰.

DNA content measurement. DNA extraction from fish swim bladders before and after decellularization was performed using a mouse tail genomic DNA kit (Kangweishiji, Jiangsu, CW2094). Briefly, fresh and decellularized swim bladders were cut into uniformly sized pieces (0.5 \times 0.5 cm) and placed in a centrifuge tube. Five-hundred microliters of prepared lysate (5 μ L of Proteinase K at 10 mg/mL) was added to each tube, and the tubes were placed in a 55 °C water bath and incubated overnight. The tubes were centrifuged at 13,000 rpm at room temperature for 15 min. Four-hundred microliters of supernatant was pipetted into a new tube, and an equal volume of isopropanol was added and mixed well. The tubes were then centrifuged at 12,000 rpm for 10 min at room temperature. The tubes were air dried on an ultra-clean table for about 3–5 min. The contents were resuspended with 80 μ L of pure water and lysed at 55 °C for 2 h; the resuspended liquid was tested using a quantitative DNA (Thermo scientific, Nanodrop 2000) assay.

Cell culture. Human umbilical vein endothelial cells (HUVEC, ECV304, Oligobio Co.Ltd., Beijing, China) of the 3rd to the 5th passages were seeded on the sterile decellularized fish swim bladder and coated decellularized fish swim bladder (swim bladders were sterilized with 75% alcohol for 12 h) with a density of 1.5×10^4 cells/mL, and cultured in 5% CO₂ and 37 °C for 4 h or 3 days. Then, the EC were stained with Acridine orange (AO) and Ethidium bromide (EB), and observed under fluorescence microscopy (Ti, Nikon, Japan). The percentage of viable cells (vital ratios) of EC on each sample were counted and calculated from 15 random visual fields. After treating with 4% paraformaldehyde for 1 h at room temperature, the EC were stained with phalloidin and 4,6-diamino-2-phenylindole (DAPI), and the number of EC on each surface were also counted⁴⁷.

Animal model. Male Sprague Dawley (SD) rats (6–8-week old) were used for all the animal experiments. Anesthesia was given via inhaled isoflurane, and adequate anesthesia was confirmed through a lack of reaction to a toe and tail pinch; ointment on the eyes was placed to prevent dryness while the animals were under anesthesia, and the ventral abdomen hair was removed using a hair remover while wearing sterile gloves. For postoperative analgesia, buprenorphine was given at 0.1 mg/kg intramuscularly no less than every 12 h for 24 h following the surgical procedures. The status of the animal was checked every day in the animal room, ensuring proper recovery from the peri-operative period as well as adequate treatment of post-surgical pain. All the animal models in this research were performed by a skilled vascular surgeon (Dr. Hualong Bai).

The aorta and inferior vena cava patch angioplasty models were performed²⁸, microsurgical procedures were performed aseptically using a dissecting microscope (Nikon, Japan). Briefly, the rat abdominal aorta was exposed and dissected free of surrounding structures, and the infrarenal aorta was clamped; a longitudinal 3 mm arteriotomy was then made on the anterior aortic wall, and a control (decellularized but uncoated) or rapamycin-coated swim bladder patch (3 × 1 mm) was sutured in place using running 10-0 nylon sutures. After completion of the angioplasty, the micro clamps were removed and aortic flow was restored. The abdomen was then closed using 5-0 Dacron sutures. The inferior vena cava (IVC) patch venoplasty model was performed using a similar procedure on the IVC (Fig. 1). Rats were sacrificed on postoperative day 14 and the patches were explanted for analysis. To avoid confounding or off-target effects, no immunosuppressive agents, antibiotics, antiplatelet agents, or heparin were given at any time during or after the operative procedure.

The aorta and inferior vena cava interposition models were performed^{48,49}. The swim bladder tissue sheets were formed into a tube configuration (inner diameter 1.0 mm for aorta or 2.0 mm for IVC; length 3–5.0 mm; measured directly with a ruler) using 11-0 sutures. The abdominal aorta below the renal artery was exposed and dissected; the proximal and distal aorta were clamped and the aorta transected. The graft was then sutured with an end-to-end configuration using a running 11-0 sutures. The IVC interposition graft was carried out in a similar fashion. Rats were sacrificed on postoperative days 14 and the patches were explanted for analysis; since we found that neointimal hyperplasia was consistent after day 7 in our previous studies^{23,29,38}, we chose day 14 as the observational time point^{25,26,27}. No immunosuppressive agents, antibiotics, antiplatelet agents, or heparin were given at any time.

At predetermined times the patch and tube grafts were harvested; the rat was anesthetized, the chest was opened, the left ventricle was cannulated with a blunted 20-gauge needle connected to a 20-mL syringe, and an incision was made in the right atrium to allow outflow of perfusion solutions; 100 mL of phosphate-buffered saline (PBS) was infused followed by 10% formalin was perfused by manual pulsatile syringe pressure. The patch or tube graft was carefully removed from the surrounding tissue and stored in 4% neutral buffered formaldehyde.

For the subcutaneous and abdominal cavity implantation models, the control decellularized and rapamycin-coated fish swim bladder patches were implanted subcutaneously and into the abdominal cavity. Patches were harvested at day 1, day 3 or day 7 for analysis.

Nanoparticle-rhodamine (NP-rhodamine) patches were also implanted either subcutaneously or into the abdominal cavity, and then harvested at 6, 12 or 24 hours²³.

Histology and EVG staining. Rats were anesthetized with 10% chloral hydrate (intraperitoneal injection), and tissues were fixed by transcardial perfusion of phosphate-buffered saline (PBS) followed by 10% formalin. Tissue was removed and fixed overnight in 10% formalin followed by a 24-h immersion in 70% alcohol. Tissue was then embedded in paraffin and sectioned (4 μm thickness). Tissue sections were deparaffinized and stained with hematoxylin and eosin (Baso, Zhuhai, China), EVG (Baso, Zhuhai, China), trichrome masson (Baso, Zhuhai, China), Alizarin Red S (Solarbio, Beijing, G3280), Safranin O (Solarbio, Beijing, G1371), or Sirius Rosa BB (Solarbio, Beijing, S8060) according to the manufacturer's recommendations. Neointimal and adventitial thickness were measured as we previously described³⁸. The patency of the patch angioplasty and tube graft was confirmed by observation of the histology sections.

Immunofluorescence. Tissue sections were deparaffinized and then incubated with primary antibodies overnight at 4 °C. The sections were incubated with

secondary antibodies for 1 h at room temperature, after which sections were stained with the fluorescent dye 40,6-diamidino-2-phenylindole (Solarbio, Beijing, China) to mark cellular nuclei. Rhodamine conjugated patches were processed as described above and observed directly under the fluorescence microscope.

Antibodies. Primary antibodies included: anti-CD68 (abcam, ab31360; IF, 1:50); anti-CD31 (R&D, AF3628; IHC, 1:100); anti-α-actin (abcam, ab5694; IF, 1:200); anti-IL-10 (abcam, ab9969; IF, 1:100); anti-iNOS (abcam, ab15323; IF, 1:100); anti-TGM2 (abcam, ab421; IF, 1:100); anti-TNF-α (abcam, ab6671; IF, 1:100); anti-CD34 (abcam, ab81289; IF, 1:50); anti-Ephrin-B2 (Abclon, A5669; IHC, 1:50); anti-Eph-B4 (proteintech, 20883-1-AP; IHC, 1:50); anti-dll4 (Abclon, A12943; IHC, 1:50); anti-COUP TF II (Abclon, A10251; IHC, 1:50). Secondary antibodies used for IF were from Abclonal, Wuhan, China.

Statistics and reproducibility. Data are expressed as the mean ± SEM. Statistical significance for these analyses was determined by one-way ANOVA and Tukey's multiple comparisons test, or *t*-tests (Prism 6; GraphPad Software, La Jolla, CA). *p*-values < 0.05 were considered significant. Animals or independent experiments (*n*) are indicated in the figure legend. Data, expressed as mean ± standard error of mean (s.e.m.), showed high reproducibility between replicate experiments (< 10% variation).

Reporting summary. Further information on research design is available in the Nature Research Reporting Summary linked to this article.

Data availability

Source data underlying all the main graphs illustrated in this manuscript are available in the Supplementary Data file.

Received: 5 April 2021; Accepted: 18 September 2021;

Published online: 05 October 2021

References

- Jafarihaghighi, F., Ardjmand, M., Mirzadeh, A., Hassani, M. S. & Parizi, S. S. Current challenges and future trends in manufacturing small diameter artificial vascular grafts in bioreactors. *Cell Tissue Bank*. **21**, 377–403 (2020).
- Giswold, M. E. et al. Modifiable patient factors are associated with reverse vein graft occlusion in the era of duplex scan surveillance. *J. Vasc. Surg.* **37**, 47–53 (2003).
- De Bakey, M. E., Cooley, D. A., Crawford, E. S. & Morris, G. C. Jr Clinical application of a new flexible knitted dacron arterial substitute. *Am. Surg.* **24**, 862–869 (1958).
- Johnson, J. M., Goldfarb, D. & Baker, L. D. Jr Expanded polytetrafluoroethylene as a small artery replacement. A preliminary report. *Am. J. Surg.* **132**, 723–727 (1976).
- Veith, F. J. et al. Six-year prospective multicenter randomized comparison of autologous saphenous vein and expanded polytetrafluoroethylene grafts in infrainguinal arterial reconstructions. *J. Vasc. Surg.* **3**, 104–114 (1986).
- Deb, S. et al. SUPERIOR SVG: no touch saphenous harvesting to improve patency following coronary bypass grafting (a multi-Centre randomized control trial, NCT01047449). *J. Cardiothorac. Surg.* **14**, 85 (2019).
- Bai, H. et al. Adult Human Vein Grafts Retain Plasticity of Vessel Identity. *Ann. Vasc. Surg.* **68**, 468–475 (2020).
- Boren, C. H., Roon, A. J. & Moore, W. S. Maintenance of viable arterial allografts by cryopreservation. *Surgery* **83**, 382–391 (1978).
- Dardik, H. & Dardik, II. Successful arterial substitution with modified human umbilical vein. *Ann. Surg.* **183**, 252–258 (1976).
- Field, P. L. The chemically treated bovine ureter—clinical performance of a novel biological vascular prosthesis. *Cardiovascular Surg.* **11**, 30–34 (2003).
- Katzman, H. E., Glickman, M. H., Schild, A. F., Fujitani, R. M. & Lawson, J. H. Multicenter evaluation of the bovine mesenteric vein bioprostheses for hemodialysis access in patients with an earlier failed prosthetic graft. *J. Am. Coll. Surg.* **201**, 223–230 (2005).
- Heine, J. et al. Tissue engineering human small-caliber autologous vessels using a xenogenous decellularized connective tissue matrix approach: preclinical comparative biomechanical studies. *Artif. organs* **35**, 930–940 (2011).
- Bader, A. et al. Engineering of human vascular aortic tissue based on a xenogeneic starter matrix. *Transplantation* **70**, 7–14 (2000).
- Niklason, L. E. & Lawson, J. H. Bioengineered human blood vessels. *Science* **370**, <https://doi.org/10.1126/science.aaw8682> (2020).
- Sung, Y. K. & Kim, S. W. Recent advances in polymeric drug delivery systems. *Biomater. Res.* **24**, 12 (2020).
- Zhao, W. H., Chi, C. F., Zhao, Y. Q. & Wang, B. Preparation, physicochemical and antioxidant properties of acid- and pepsin-soluble collagens from the

- swim bladders of miyu croaker (*Miichthys miiuy*). *Marine Drugs* **16**, <https://doi.org/10.3390/md16050161> (2018).
17. Sousa, R. O. et al. Acid and enzymatic extraction of collagen from Atlantic cod (*Gadus Morhua*) swim bladders envisaging health-related applications. *J. Biomater. Sci. Polym. Ed.* **31**, 20–37 (2020).
 18. Kumar, V., Kumar, N., Gangwar, A. K., Singh, H. & Singh, R. Comparative histologic and immunologic evaluation of 1,4-butanediol diglycidyl ether crosslinked versus noncrosslinked acellular swim bladder matrix for healing of full-thickness skin wounds in rabbits. *J. Surgical Res.* **197**, 436–446 (2015).
 19. Morris, S. M. & Albright, J. T. Ultrastructure of the swim bladder of the goldfish, *Carassius auratus*. *Cell Tissue Res.* **198**, 105–117 (1979).
 20. Liu, J. et al. Swim bladder as a novel biomaterial for cardiovascular materials with anti-calcification properties. *Adv. Healthc. Mater.* **9**, e1901154 (2020).
 21. Radke, D. et al. Tissue engineering at the blood-contacting surface: a review of challenges and strategies in vascular graft development. *Adv. Healthc. Mater.* **7**, e1701461 (2018).
 22. AbuRahma, A. et al. The use of drug-eluting stents in patients with critical limb ischemia and infrapopliteal arterial disease a real world single center experience. *J. Vasc. Surg.* <https://doi.org/10.1016/j.jvs.2021.06.019> (2021).
 23. Bai, H. et al. Covalent modification of pericardial patches for sustained rapamycin delivery inhibits venous neointimal hyperplasia. *Sci. Rep.* **7**, 40142 (2017).
 24. Bai, H. et al. Application of the tissue-engineered plant scaffold as a vascular patch. *ACS Omega* **6**, 11595–11601 (2021).
 25. Bai, H. et al. Hyaluronic acid-heparin conjugated decellularized human great saphenous vein patches decrease neointimal thickness. *J. Biomed. Mater. Res. Part B, Appl. Biomater.* **108**, 2417–2425 (2020).
 26. Bai, H. et al. Inhibition of programmed death-1 decreases neointimal hyperplasia after patch angioplasty. *J. Biomed. Mater. Res. Part B, Appl. Biomater.* **109**, 269–278 (2021).
 27. Sun, P. et al. Programmed death-1 mediates venous neointimal hyperplasia in humans and rats. *Aging (Albany NY)* **13**, 16656–16666 (2021).
 28. Bai, H. et al. Patch Angioplasty in the Rat Aorta or Inferior Vena Cava. *J. Vis. Exp.* <https://doi.org/10.3791/55253> (2017).
 29. Bai, H. et al. Polyester vascular patches acquire arterial or venous identity depending on their environment. *J. Biomed. Mater. Res. Part A* **105**, 3422–3431 (2017).
 30. Goel, S. A., Guo, L. W., Liu, B. & Kent, K. C. Mechanisms of post-intervention arterial remodelling. *Cardiovascular Res.* **96**, 363–371 (2012).
 31. Boada, C. et al. Rapamycin-loaded biomimetic nanoparticles reverse vascular inflammation. *Circ. Res.* **126**, 25–37 (2020).
 32. Danenberg, H. D. et al. Systemic depletion of macrophages by liposomal bisphosphonates reduces neointimal formation following balloon-injury in the rat carotid artery. *J. Cardiovasc. Pharm.* **42**, 671–679 (2003).
 33. Wolff, R. A. et al. Macrophage depletion reduces monocyte chemotactic protein-1 and transforming growth factor-beta1 in healing rat vein grafts. *J. Vasc. Surg.* **39**, 878–888 (2004).
 34. Du, L. J. et al. Macrophage NCOR1 deficiency ameliorates myocardial infarction and neointimal hyperplasia in mice. *J. Am. Heart Assoc.* **9**, e015862 (2020).
 35. Lavin, B. et al. Nitric oxide prevents aortic neointimal hyperplasia by controlling macrophage polarization. *Arterioscler. Thromb. Vasc. Biol.* **34**, 1739–1746 (2014).
 36. Inoue, T. et al. Vascular inflammation and repair: implications for re-endothelialization, restenosis, and stent thrombosis. *JACC Cardiovasc. Inter.* **4**, 1057–1066 (2011).
 37. Ma, X. et al. Delayed re-endothelialization with rapamycin-coated stents is rescued by the addition of a glycogen synthase kinase-3beta inhibitor. *Cardiovascular Res.* **86**, 338–345 (2010).
 38. Bai, H. et al. Pericardial patch venoplasty heals via attraction of venous progenitor cells. *Physiol. Rep.* **4**, <https://doi.org/10.14814/phy2.12841> (2016).
 39. Bai, H. et al. Transforming growth factor-beta1 inhibits pseudoaneurysm formation after aortic patch angioplasty. *Arterioscler. Thromb. Vasc. Biol.* **38**, 195–205 (2018).
 40. Devine, C., McCollum, C. & North West Femoro-Popliteal Trial, P. Heparin-bonded Dacron or polytetrafluorethylene for femoropopliteal bypass: five-year results of a prospective randomized multicenter clinical trial. *J. Vasc. Surg.* **40**, 924–931 (2004).
 41. Copes, F., Pien, N., Van Vlierberghe, S., Boccafroschi, F. & Mantovani, D. Collagen-based tissue engineering strategies for vascular medicine. *Front. Bioeng. Biotechnol.* **7**, 166 (2019).
 42. Bai, H., Dardik, A. & Xing, Y. Decellularized carotid artery functions as an arteriovenous graft. *J. Surgical Res.* **234**, 33–39 (2019).
 43. Li, J. et al. Controlling molecular weight of hyaluronic acid conjugated on amine-rich surface: toward better multifunctional biomaterials for cardiovascular implants. *ACS Appl. Mater. Interfaces* **9**, 30343–30358 (2017).
 44. Li, J., Zhang, K. & Huang, N. Engineering cardiovascular implant surfaces to create a vascular endothelial growth microenvironment. *Biotechnol. J.* **12**, <https://doi.org/10.1002/biot.201600401> (2017).
 45. Wang, S., Zhu, S. J., Zhang, X. Q., Li, J. A. & Guan, S. K. Effects of degradation products of biomedical magnesium alloys on nitric oxide release from vascular endothelial cells. *Med. Gas. Res.* **9**, 153–159 (2019).
 46. Pensalfini, M. et al. The suture retention test, revisited and revised. *J. Mech. Behav. Biomed. Mater.* **77**, 711–717 (2018).
 47. Li, J. A., Chen, L., Zhang, X. Q. & Guan, S. K. Enhancing biocompatibility and corrosion resistance of biodegradable Mg-Zn-Y-Nd alloy by preparing PDA/HA coating for potential application of cardiovascular biomaterials. *Mater. Sci. Eng. C. Mater. Biol. Appl.* **109**, 110607 (2020).
 48. Luo, J. et al. Tissue-engineered vascular grafts with advanced mechanical strength from human iPSCs. *Cell Stem Cell* **26**, 251–261 e258 (2020).
 49. Fukunishi, T. et al. Different degradation rates of nanofiber vascular grafts in small and large animal models. *J. Tissue Eng. Regen. Med.* **14**, 203–214 (2020).

Acknowledgements

This study was funded by the National Natural Science Foundation of China to Hualong Bai (Grant No: 81870369) and Key Projects of Medical Science and Technology in Henan Province to Hualong Bai (Grant No: SBGJ202002035).

Author contributions

H.B., J.L., A.D., and Z.L. designed experiments, performed data analysis, wrote, and revised the manuscript; H.B., P.S., H.W., and S.W. conducted animal studies, histological experiments, W.W., Y.H., B.X., and J.L. compiled data; and H.B. obtained funding.

Competing interests

The authors declare no competing interests.

Additional information

Supplementary information The online version contains supplementary material available at <https://doi.org/10.1038/s42003-021-02696-9>.

Correspondence and requests for materials should be addressed to Hualong Bai, Jing'an Li, Alan Dardik or Zhuo Li.

Peer review information *Communications Biology* thanks Bo Wang and the other, anonymous, reviewers for their contribution to the peer review of this work. Primary Handling Editors: Ngan Huang and Caitlin Karniski.

Reprints and permission information is available at <http://www.nature.com/reprints>

Publisher's note Springer Nature remains neutral with regard to jurisdictional claims in published maps and institutional affiliations.



Open Access This article is licensed under a Creative Commons Attribution 4.0 International License, which permits use, sharing, adaptation, distribution and reproduction in any medium or format, as long as you give appropriate credit to the original author(s) and the source, provide a link to the Creative Commons license, and indicate if changes were made. The images or other third party material in this article are included in the article's Creative Commons license, unless indicated otherwise in a credit line to the material. If material is not included in the article's Creative Commons license and your intended use is not permitted by statutory regulation or exceeds the permitted use, you will need to obtain permission directly from the copyright holder. To view a copy of this license, visit <http://creativecommons.org/licenses/by/4.0/>.

© The Author(s) 2021